Aqueous secondary organic aerosol formation in ambient cloud water photo-oxidations

M.I. Schurman[1,2*], A. Boris[1], Y. Desyaterik[1], J. L. Collett, Jr.[1]

[1]*Department of Atmospheric Science, Colorado State University, Fort Collins, CO, 80521, USA*

[2]*Colorado Mountain College, Breckenridge, CO, 80424, USA*

Abstract

The current understanding of aqueous secondary organic aerosol (aqSOA) formation is based largely on laboratory investigations of very simple surrogate cloud water solutions that aid mechanistic understanding of aqueous oxidation but may not accurately reflect the influence of the complex ambient matrix present in authentic cloud waters on organic chemistry. In this study, unaltered ambient cloud water and 'biogenically influenced' ambient cloud water (with added pinonic acid) were photo-oxidized, atomized, and dried to simulate the formation of aqSOA in clouds, then analyzed using an Aerodyne Aerosol Mass Spectrometer. Two major chemical regimes were identified: in the first, particle organic mass is gained, then lost; sustained increases in highly oxidized fragments indicate overall organic acid formation, while increases in nominally volatile fragments suggest that evaporation may contribute to the observed mass decrease. In the second regime, the oxidation level of cloud water organic matter decreases as mass decreases, suggesting that oxidized functional groups are fragmented and lost to evaporation. Overall, the rate of aqSOA production in unaltered cloud water decreases as oxygenation increases, until organic mass loss beginning at consistent values of $f44 > 0.23 \pm 0.05$ and O:C $> 0.61 \pm 0.05$. We hypothesize that there may be a parameterizable 'maximum oxidation level' for cloud water above which functional group fragmentation is dominant. These experiments are among the first to quantify organic mass production in ambient cloud water and employ the most atmospherically relevant oxidant concentrations to date.

Keywords: Secondary organic aerosol; Cloud chemistry; Photooxidation; Aqueous.

* Corresponding author. Tel: 1-720-485-9191
E-*mail address*: mishaschurman.ms@gmail.com

INTRODUCTION

Particles in the atmosphere have wide-ranging health, environmental, and climate effects, many of which are attributed disproportionately to fine-mode (<2.5μm diameter) secondary organic aerosols (SOA). While gas-phase chemistry and subsequent partitioning was traditionally thought to be the main source of SOA, this mechanism fails to predict the amount, content (Chang and Thompson, 2010), distribution (Heald et al., 2005; Tsigaridis & Kanakidou, 2003), and size of ambient particles (Blando and Turpin, 2000), where 'ambient particles' are defined as particles found in ambient air; recent work suggests that up to ~50% of total SOA mass is formed through aqueous reactions (Ervens et al. 2011). However, most of our knowledge of SOA formation is based on laboratory investigations of very simple solutions that aid mechanistic understanding of aqueous oxidation but may not accurately reflect the influence of the complex ambient matrix (defined as the mixture of compounds comprising a cloud water sample) on organic chemistry (Boris et al., 2014). This paper seeks to investigate the relevance of previous aqueous SOA (aqSOA) studies by photo-oxidizing ambient cloud water (defined as cloud water collected in-situ from natural clouds) with and without addition of common aqSOA precursors; while the complexity of the cloud water matrix prevents precise mechanistic determination, general reaction regimes may be inferred in terms of changes in organic mass, composition, and level of oxidation. Such an approach can be very useful, especially given our incomplete understanding of the organic composition of ambient aerosols and cloud water.

Important aqSOA precursors include anthropogenic and biogenic volatile organic compounds (A- and B-VOCs, respectively) oxidized to form products such as glyoxal, methylglyoxal, pinonaldehyde, and pinic/pinonic acids (Fu et al., 2008; Atkinson and Arey, 2003). Pinonic acid is used herein to represent oxidation products of α-pinene which may be absorbed from cloud interstitial spaces (Jang, 1999; Kanakidou et al., 2005), as a proxy for

74 total interstitial BVOC absorption. We hypothesize that this addition of organic material, and
75 its relatively low oxidation level relative to the original cloudwater, may augment and/or
76 sustain aqSOA formation as found in the previous works (see discussion in Results Section).
77 The hydroxyl radical (OH) is a dominant aqueous oxidant (Herrmann et al., 2010). OH
78 can be absorbed from the gas phase, but is also formed significantly (up to ~33%; Ervens et
79 al. 2003; Arakaki & Faust 1998) by aqueous photolysis of hydrogen peroxide (H_2O_2; Zellner
80 et al. 1990; Graedel & Goldberg 1983), iron(III) hydroxide ($Fe(OH)^{2+}$; Arakaki and Faust,
81 1998; Weschler et al., 1986), nitrous acid (HONO; Arakaki and Faust, 1998; Fischer and
82 Warneck, 1996), and nitric acid (HNO_3; Graedel and Weschler, 1981); H_2O_2 and HO_x (HO+
83 hydroperoxyl radical, HO_2) may also undergo regenerative chemistry involving organic
84 radicals (Anastasio et al., 1994; Valverde-Canossa et al., 2005). Direct organic photolytic
85 oligomerization and lysing reactions are also possible and may form OH in turn through HO_x
86 cycling, though organic radical-initiated reactions are generally not competitive with OH
87 oxidation (Guzman et al., 2006, Tan et al. 2010; Tan et al. 2012). Fenton reactions may
88 produce OH in the absence of ultraviolet light (UV; Arakaki and Faust, 1998; Deguillaume et
89 al., 2005), which motivated our no-UV control experiments. Reaction with OH and
90 photolysis are important aqueous pinonic acid sinks (Lignell et al., 2013).
91 The current understanding of aqSOA mechanisms, products, and yields is based largely
92 on laboratory investigations of simple solutions with unrealistically high oxidant and reactant
93 concentrations. Solute concentration strongly influences aqSOA yield and product type, with
94 higher concentrations forming higher molecular weight compounds such as oligomers
95 through organic self-reaction, while lower fog- and cloud-relevant concentrations often form
96 organic acids (Lim et al. 2010; Tan et al. 2009). Solute composition is also important, as
97 organic radical formation, hygroscopicity, acidity, and component distribution in the droplet
98 (e.g. organic shells) may all affect aqSOA yields (Ervens and Volkamer, 2010; Galloway et

al., 2011; Volkamer et al., 2009).

Simple solutions of common SOA precursors, while more mechanistically constrained, may not accurately represent the complex chemistry in real atmospheric waters. This work explores how photooxidation influences ambient cloud water organic mass, average oxidation state, and reaction regimes (such as functionalization versus fragmentation), and investigates relationships between oxidative progression and solution characteristics such as total organic carbon (TOC) and oxidation level (oxygen-to-carbon elemental ratios (O:C), *f*44, etc.). The experiments presented here compare bulk photo-oxidations of real cloud water and cloud water with added pinonic acid (simulating 'biogenic precursor' addition), all featuring among the most atmospherically relevant reactant and oxidant concentrations to date.

METHODS

The Aerodyne High Resolution Time-of-Flight Aerosol Mass Spectrometer (AMS) measures the size and composition of submicron non-refractory particles with high time- and mass-resolution and has been described elsewhere (Decarlo et al., 2006); vaporization and electron impact ionization therein cause molecular fragmentation, complicating identification of specific reaction products as discussed later. AMS data quality is constrained by rigorous calibration; a LI-COR LI-820 monitor before the inlet constrained $CO_{2(g)}$ contributions to the CO_2^+ fragment. The ToF-AMS DAQ v 1.7.2B software was used for data acquisition; data analysis utilized the SQUIRREL (v1.52K) and PIKA (v1.11K, Sueper et al., 2011) tools in Igor Pro 6.22A (WaveMetrics Inc., Lake Oswego, OR). Measurements near the AMS detection limit were not altered or eliminated. Particulars can be found in the supplement.

Briefly, bulk solutions are oxidized in a beaker-like vessel using UV light (Green Killing Machine, Model AAUV09W-UVC, 254 nm peak wavelength) and hydrogen peroxide, atomized (TSI 3076), dried (mimicking particle formation from cloud droplet evaporation, Lee et al. 2011; El Haddad et al. 2009; De Haan et al. 2009; Loeffler et al. 2006), and

analyzed via AMS with 1-minute time resolution after Lee et al. (2011b), with the addition of (a) a continuously circulating water sheath around the reaction vessel for temperature control at ~22 C (AquaBox fish-tank pump, Model AA2005), (b) a water trap after the atomizer (intermittent visible water at the atomizer outlet, see supplement), and (c) a ^{210}Po neutralizer between the driers and the AMS (Figure 1; Boris et al., 2014). Photo-oxidations lasted between ~30-140 minutes; control experiments ran for ~20 minutes (see supplement). Photo-reactor and stir bar were cleaned with deionized water and air-dried between each experiment.

Five ambient cloud samples from Mt. Tai, China were used (named T1-4 and T7); T7 was oxidized with (T7PA) and without (T7) added pinonic acid (30 μM). See supplement section S3 and Shen (2011) for sampling, storage, and composition details. Generally, pinonic acid (PA) concentrations in cloud water are unknown; due to similarity between yields of pinonic acid (~0.1-1%), pinic acid (~1-5%), and pinonaldehyde (~0-1%) from α- and β-pinene aqueous oxidation (Yu et al., 1999), we conjecture that ambient pinonic acid concentrations might be similar to those of pinic acid and pinonaldehyde (0.11 and 0.8 μM, respectively; van Pinxteren et al., 2005). Species concentrations are normalized by total sulfate to correct noise from fluctuating atomizer output (supplement Sections S2 and S4 for detailed methodological assessment).

Hydroxyl radicals were produced via photolysis of hydrogen peroxide (300 μM). The resulting $[OH]_{aq}$ was quantified in the cloud samples (and deionized water for comparison purposes) via absorption spectroscopy of 202 nm light by salicylic acid, which was below detection limit in the cloud samples, preceded by reverse phase liquid chromatography separation to prevent measurement interference from other absorbing species (N=3; accounting for salicylic acid direct photolysis and using the second-order rate constant of 1.6×10^{10} $M^{-1}s^{-1}$; see Boris et al., 2014); these measurements yielded 1.9×10^{-14} M OH within the cloud water and $5.4 \pm 0.5 \times 10^{-14}$ M OH within pure water (Boris et al., 2014).

Before hydrogen peroxide addition, these ambient cloud samples contained $[HOOH]_{aq}$ = 1-100 μM (Shen 2011); assuming that the rate constant for OH production by hydrogen peroxide photolysis used herein holds in the complex ambient matrix, and that OH-organic reaction rate increases are linear within the given [OH] concentration range, this initial hydrogen peroxide content produces concentrations of $[OH]_{aq} \approx 10^{-15}$– 10^{-14} M which, adding the supplementary hydrogen peroxide, yields $[OH]_{aq} \approx 10^{-14}$ M. Ambient cloud [OH] is difficult to measure, but has been estimated at ~10^{-14} to 10^{-13} M (Arakaki & Faust 1998; Ervens et al. 2003; Ervens & Volkamer 2010; Jacob 1986; Deguillaume et al. 2005), 1-2 orders of magnitude lower than used in similar laboratory experiments (Lim et al. 2010; Lee et al. 2011a). These solutions are among the most atmospherically relevant used in the laboratory to date; methodological assessment of evaporative cycling effects and OH exposure is discussed further in supplement Section S4.

RESULTS

Control Experiments

Control experiments evaluated contributions of dark (noUV/noH_2O_2, 'baseline'), photolytic (+UV/noH_2O_2), and hydrogen peroxide-initiated (noUV/+H_2O_2) reactions to aqSOA. For ambient cloud samples from Mt. Tai, China (T1-T7), neither organic mass (Total Organics/Total Sulfate, normalized to t = 0) nor oxidation indicator *f*44 (mass at *m/z* 44/Total Organics, normalized to t = 0) change significantly under any of the control conditions, indicating probable dominance of OH-initiated reactions in the full photo-oxidations (Figure S1).

Ambient Cloud Water Photo-oxidation

Organic mass (Org/SO_4), O:C, and *f*44 (*m/z* 44/Org) for ambient cloud water photo-oxidation experiments are shown in Figure 2; sample volume limited the duration of T1. Figure 3 shows timelines of CO_2^+/SO_4 (Takegawa et al., 2007), $C_2H_3O^+/SO_4$ (at *m/z* 43,

178 indicating carbonyl content; McLafferty and Turecek, 1993), and $C_2H_3O^+/C_4H_7^+$ (ratio of
179 most to least oxidized fragment at *m/z* 43), as well as $CH_2O_2^+/SO_4$, which is, nominally,
180 formic acid (a major oxidation product of glyoxal compounds; see supplement S4 for caveats
181 to formic acid quantification via AMS). Although determination of specific oxidative
182 mechanisms is precluded by both fragmentation in the AMS and the complexity of the
183 ambient cloud water composition, possible functionalization pathways are examined using
184 delta analysis and movement in van Krevelen space.

185 Experiments may be grouped according to their oxidative behavior into two groups. In
186 Functionalization-Dominant Regime 1 (T1 and T3) samples first gain, then lose organic mass,
187 and gain, then sustain CO_2^+ fragments & *f*44 representing carboxylic acids (and other
188 oxygenated fragments, as seen in difference spectra Figure S4) indicating retention of
189 oxygenated products. In contrast, in Fragmentation-Dominant Regime 2 (T4 and T7), organic
190 mass is unchanging for the first 30-60 minutes and decreasing significantly thereafter; there is
191 no increase in organic mass as seen in Regime 1. Additionally, there is early formation, then
192 pronounced loss of oxygenated fragments; together, these suggest mass loss due to
193 functional-group fragmentation. Evidence supporting these regime groupings is detailed in
194 the following sections.

195 ***Functionalization-Dominant Regime 1: Oxygenated products maintained***

196 For the T1 and T3 experiments with ambient Mt. Tai cloud water, Org/SO_4 increases
197 for the first 15-30 minutes (to ~110% and ~140% of the t = 0 value, respectively), then
198 decreases for the remainder of the experiment. Oxidation proxy *f*44 and carboxylic acid
199 indicator CO_2^+/SO_4 increase for the first 15-30 minutes (T1 and T3); the T3 experiment ran
200 longer and these proxies were observed to stay constant thereafter through 90 minutes.
201 Reduction in $C_2H_3O^+/SO_4$ beginning at ~10 min may result from oxidation of carbonyls to
202 carboxylic acids; contemporaneous rapid oxidation of C_xH_y species is indicated by an

increase in $C_2H_3O^+/C_4H_7^+$ (from ~10-25 minutes in T1 and ~6-16 minutes in T3), indicating that $C_4H_7^+$ must be decreasing faster than $C_2H_3O^+$. After ~10-15 minutes, both $C_2H_3O^+/SO_4$ and $C_2H_3O^+/C_4H_7^+$ decrease, indicating a net loss of hydrocarbons and carbonyls. Most chemical change discernable via AMS occurs in the first half-hour or so of oxidation.

A picture emerges of rapid oxidation of hydrocarbons to carbonyls and carbonyls to carboxylic acids, consistent with other similar studies (Lee et al., 2011a). This is supported by difference spectra for the major organic fragment 'families' (CH, CHO, $CHO_{n>1}$; Figure S4), in which CH fragments decrease and CHO and $CHO_n>1$ generally increase, especially at *m/z* 44 (CO_2^+); slight decreases in some CHO fragments commensurate with increases in $CHO_{n>1}$ fragments at the same *m/z* reflect oxidation of carbonyls to carboxylic acids. These patterns can also be seen in delta mass spectral analysis (see supplement S6 and discussion below).

The 'formic acid' fragment increases in both T1 and T3, suggesting that volatile formic acid and/or molecules fragmenting to $CH_2O_2^+$ are early-generation products. Formic acid production occurs in aqueous oxidations of glyoxal and is responsible for the eventual loss of total organic mass in those experiments due to its volatility and resultant loss during drying (Lee et al. 2011b); the same mechanism could also be at play in T1 and T3, accompanied by decomposition of oxidized molecules to hydrocarbons and other non-formic-acid volatile fragments that are lost during evaporation as evidenced above.

Fragmentation may be further explored through the slope of movement in van Krevelen space (O:C vs H:C, see Figure 4) as an isolated particle/droplet population reacts (e.g. Heald et al. 2010). T1 and T3, though with different compositions and therefore different starting positions in the diagram, move similarly toward enhanced O:C with slopes near -0.3, which is between m=-0.5, indicative of either carboxylic addition with C-C bond breakage or addition of both acid and alcohol/peroxide functional groups without fragmentation (total 1 H loss per

2 O addition, Figure 4), and m=0, indicative of alcohol or peroxide addition. Delta analysis can reveal which of these mechanisms are important (see supplement S6), as functional group composition dictates fragment *m/z* values such that delta (Δ) = *m/z* - 14*n* + 1, where *n* is the number of methylene (CH_2) bridges on the functional group (Table S3, McLafferty and Turecek, 1993). For T1 and T3, reductions in Δ_{-2}, Δ_0, and Δ_6, which may be partially attributed to alcohols (Table S3), suggests at least that alcohol addition does not exceed consumption of unsaturated hydrocarbons and carbonyls (at Δ_0, Δ_{-2}), and implies that carboxylic addition with C-C fragmentation is a more important reaction pathway for this dataset; this fragmentation may also contribute to the organic mass loss observed if the non-functionalized fragments are volatile. These slopes are similar to gas-phase chamber oxidations of both generated and ambient OA (Chhabra et al., 2011; Lambe et al., 2011; Ng et al., 2011).

In contrast to experiments T1 and T3, there is relatively little change in composition during oxidation of T2. Org/SO_4 is unchanging for the first ~20 minutes, with subsequent decrease (Figure 2). *f*44 increases slightly, but given that CO_2^+/SO_4 and $C_2H_3O^+$/SO_4 are constant (statistically, with a slight CO_2^+/SO_4 decrease toward the end), this is more a function of total organic mass loss than proportional gains at *m/z* 44; $C_2H_3O^+$/$C_4H_7^+$ increases in the first ~20 minutes, indicating decrease in hydrocarbon $C_4H_7^+$, which is echoed in general (though not universal) C_xH_y reduction in the difference mass spectrum (Figure S4). However, clear progression toward higher O:C in the van Krevelen diagram (Figure 4) implies that oxygenated compounds are gained; family difference spectra reveal increases in fragments >*m/z* 50 from the oxidized $CHO_{n>1}$ family, though fragment abundance changes are small compared to the other experiments. The progression to highly oxidized ($CHO_{n>1}$) fragments > *m/z* 50 and decreased CO_2^+ suggests higher product stability against fragmentation within the AMS. By all measures, T2 started at a higher level of oxidation than

253 the other experiments, which may reduce its ability to participate in further oxidation
254 reactions, if, as discussed later, there exists a 'maximum' level of average solution oxidation
255 above which subsequent organic mass formation is hindered.

256 ***Fragmentation-Dominant Regime 2: Oxygenated fragments lost***

257 In Mt. Tai cloud water experiments T4 and T7, organic mass is unchanging for the first
258 30-60 minutes and decreasing significantly thereafter; there is no increase in organic mass.
259 Figure 2 shows that the normalized amount of Org/SO4 does not increase as in Regime 1, but
260 only decreases after the beginning of photooxidation at t=0. There is some 'noise' in this data,
261 which is discussed thoroughly in Supplement Section S2: *Description of variable atomizer*
262 *output*; nonetheless, the normalized Org/SO4 value begins to fall below 1 immediately after
263 t=0 and 'noise' does not exceed 1.09 in either T4 and T7, nor does it show the clear
264 increasing, then decreasing trends seen in T1 and T3. This is in contrast to maximum
265 normalized Org/SO4 of 1.43 and 1.12 in T3 and T1.

266 O:C and *f*44 generally increase for the first 15-30 minutes and then decrease (Figure 2).
267 T4 and T7 show early formation, then pronounced loss (beginning at ~35-40 min) of
268 CO_2^+/SO_4; the first half-hour looks similar to Regime 1 (T1 and T3), with fragment ratios
269 indicating progressive carbonyl, then carboxylic acid increases (as above), but is followed by
270 strong decreases in $C_2H_3O^+$ (to ~50% of t=0 value in T4) and CO_2^+ (max ~200% at t=20 min
271 in T4; back to starting value by experiment's end). This is in clear contrast to Regime 1, in
272 which oxygenated products were sustained throughout the experiments. The formic acid
273 fragment is near zero in T4 and with some mass in T7, but shows no significant trend in
274 either time series. The fragment-family difference spectra show universal hydrocarbon (CH)
275 loss and decreased $C_2H_3O^+$ (*m/z* 43), with small increase or decrease in experiment-end CO_2^+
276 in T4 and T7, respectively, consistent with the fragment timelines.

In the van Krevelen diagram, T4 and T7 initially progress toward higher O:C and lower H:C as would be expected of the carbonyl and carboxylic acid formation inferred from the fragment ratios above, but then move back toward lower O:C and higher H:C as photo-oxidation progresses; along with the loss of organic mass and oxygenated fragments, this suggests that oxidized functional groups are chemically fragmented in solution and lost during atomization/drying, leaving behind the hydrocarbon 'backbones' of the molecules.

Ambient Cloud Water Photo-oxidations with Added Pinonic Acid Precursor

In contrast to T7 and the other cloud samples, aqueous photo-oxidation of T7PA (T7 with added pinonic acid) has fairly constant Org/SO_4, *f*44, and CO_2^+/SO_4 (Figures 2 & 3). $C_2H_3O^+$/$C_4H_7^+$ and moderate $C_2H_3O^+$/SO_4 increases imply hydrocarbon loss and carbonyl gains that are corroborated in the difference spectra (Figures 3 & S4). In the van Krevelen diagram, T7PA resides in a region similar to T7 (Figure 4); T7PA's lower starting O:C implies that unaltered T7 is on average even more functionalized than pinonic acid, which contains both a carboxylic acid and a carbonyl group. While T7PA develops slightly higher O:C and lower H:C with time (Figure 4), these changes lack the amplitude and organization seen in T7 and the other samples in van Krevelen space. The family difference spectra reveal addition of CHO and $CHO_{n>1}$ fragments (including acids and carbonyls); delta analysis also indicates carbonyl formation in increasing Δ_2 (alkyls, saturated carbonyls).

T7PA differs from the unaltered sample (T7) in a number of ways. Addition of pinonic acid reduces the initial level of solution oxidation and pH, enhances formation of carbonyls and larger, more stable molecules (increased CHO and $CHO_{n>1}$ > *m/z* 50 fragments), and does not contain 'formic acid' signal; organic mass is maintained instead of decreased. This mass retention may be influenced by increasing total organic carbon (regardless of organic composition), as added PA constitutes a 57% increases in TOC for T7PA; increasing precursor concentration often results in higher mass production as hypothesized for this

experiment and discussed in the introduction. Chamber pinonic acid-OH oxidations have resulted in highly functionalized, low-volatility molecules (Müller et al., 2012) similar to unpublished pinonic acid aqueous photo-oxidations in our laboratory (identified via ESI-ToF-MS). Our observation of dominant carbonyl formation compares favorably to single-precursor pinonic acid photo-oxidations in our photoreactor (Schurman, 2014) and other aqueous *cis*-pinonic acid (Aljawhary et al., 2016) and α-pinene oxidations (Bleier and Elrod, 2013); however, α-pinene products appear to vary with OH exposures, with dominant carboxylic acid formation and little change in *f*43 under high-OH conditions (George and Abbatt, 2010), and carbonyl formation in the form of acetone, formaldehyde, formic acid, etc. under lower [OH] (Nozière et al., 1999); Lignell et al. (2013) show that direct aqueous PA photolysis is a minor mechanism. Since our precursor, pinonic acid, is a fairly early-generation α-pinene product and our equivalent OH exposure is approximately 1-to-1 with ambient exposure, our samples experience only a few hours of ageing compared to the days-to-weeks exposures in many chamber experiments that observe oxidation to carboxylic acids (which may be less relevant to cloud lifetimes, as well).

These results suggest that biogenic precursor addition may suppress or delay the oxidative mass loss of organics observed in aqueous photo-oxidations of unaltered cloud samples, and that total organic mass formation or loss may be related to the average level of solution oxidation. To investigate this, we evaluated the relationship between O:C, *f*44, and the incremental change in Org/SO_4, finding that mass decreases begin only when O:C > 0.61 ± 0.05, *f*44 > 0.23 ± 0.05 and, generally, *f*43 < ~0.08 ± 0.02 (T1 organic mass decreases occur with *f*43 steady at ~0.084, but this holds true for all other ambient-cloud experiments). Because multiple fragments of different degrees of oxidation contribute to both *m/z* 43 and 44, the *f*44 and *f*43 'break-over points' (at which organic mass begins to decrease) may not be as useful (or universal) as that of O:C.

DISCUSSION

Two patterns emerge in these ambient cloud water photo-oxidations: in the first (Functionalization-Dominant Regime 1; T1 & T3), organic mass is gained, then lost, and sustained increases in highly oxidized fragments indicate overall organic acid formation; decrease in hydrocarbon fragments and production of the potentially-volatile $CH_2O_2^+$ fragment ('formic acid,' which partitions mostly to the gas phase; see discussion below and Liu et al., 2012), suggests that volatilization of these species may contribute to mass decrease. In Fragmentation-Dominant Regime 2 experiments (T4 & T7), oxidized fragments decrease as mass decreases, indicating that oxidized functional groups are fragmented and lost to evaporation.

pH varies significantly between functionalization-dominant Regime 1 (pH~5.5-6.4) and fragmentation-dominant Regime 2 (pH~4.6-4.7; Figure 5). These pH variations may drive formic acid production (or at least particle partitioning, as explained below), with substantial 'formic acid' fragments occurring only in samples with pH > ~5.5 (T1 and T3); T3 had the highest pH, and also the greatest increase in nominally formic acid fragments, while T1 had a lower pH and lower formic acid concentrations. In Regime 2, for which solution pH values were ≤ 4.74, little or no formic acid was detected. This is logical, since the Henry's Law partitioning of formic acid is driven toward the particle phase by higher pH (Liu et al. 2012b). Furthermore, particulate formic acid is enhanced significantly beyond the Henry's Law equilibrium in recent studies of urban-influenced particles (including one in Beijing, China; Liu et al. 2012b; Wang et al. 2007); possible explanations include varying pH between particle bulk and surface (such that bulk measurements do not capture the pH relevant to the reaction) and variability in LWC (due to varying degrees of drying over the course of our experiments; Liu et al. 2012). Also, cations such as Ca^{2+} can undergo acid-base reactions that lead to formic acid retention in the particle phase (Fornaro and Gutz, 2003; Löflund et al.,

353 2002; Malm et al., 2009); this chemistry has been indirectly evidenced in one case,
354 coincidently involving long-range transport of formic acid and dust from China (Kawamura
355 et al., 2012).

356 Initial solution O:C (ranging from 0.35-0.53) does not vary significantly between
357 Regime 1 and Regime 2, but Regime 1 reactions generally end at higher O:C (0.69-0.95,
358 versus ~0.64 for Type 2) due to retention of oxygenated functional groups. On average,
359 Regime 1 samples had higher starting concentrations of TOC, hydrogen peroxide, and other
360 solutes, which may explain the tendency toward higher functionalization and therefore mass
361 retention as described in the introduction; however, these concentration differences were not
362 significant using the Mann-Whitney-Wilcoxon rank-sum test, and samples with equivalent
363 TOC concentrations were found between the types (Figure 5). Meteorological back-
364 trajectories indicate the same source region (the heavily populated, industrial South China
365 Plain) for air masses involved in all cloud samples (Shen, 2011).

366 Because it is difficult to both collect and to fully and continuously speciate cloud water,
367 many studies use simple surrogate cloud water solutions to better constrain yields and
368 reaction pathways, impeding direct comparison of our findings to the literature. However,
369 using methods quite similar to those herein, though with higher OH concentrations, Lee et al.
370 (2012) noted that ambient cloud samples formed highly oxidized SOA similar to that found
371 in ambient aerosols, with organic mass production maxima of ~110-130% of the initial value
372 followed by decreasing mass, similar to this work (Lee et al. 2012). A model simulation of
373 rural $SOA_{(aq+g)}$ with monoterpene emissions suggested ~21-25% SOA mass increase in the
374 first ~1 hour when clouds (pH = 4.5) were added, with a slight reduction in mass after ~2
375 hours much like our experiments (Chen et al. 2007a), while urban aerosol with anthropogenic
376 emissions (NO_x, aromatics, alkanes) increased about 10% with no subsequent decrease; as in
377 this work, model addition of less oxidized precursors appeared to augment and/or sustain

aqSOA increases, supporting the hypothesis that pinonic acid addition would do the same. This hypothesis is also supported by a methacrolein cloud chamber photo-oxidation experiment involving a continuous interstitial source of less-oxidized precursors gases, which found a non-linear 47-fold increases in SOA mass sustained over a 22-hour experiment (El Haddad et al., 2009; Liu et al., 2009; Monod et al., 2007; Monod et al., 2000).

The methodology used herein does differ from ambient cloud processing in some ways. First, bulk-phase photooxidations disregard the continuous evaporation and re-condensation of cloud droplets, which influences evaporative losses and the cycling of interstitial VOCs, semi-volatile compounds, oxidants, and oxygen (O_2) through the gas and droplet phases; this may in turn change aqSOA production (De Haan et al. 2009). With typical cloud droplet lifetimes of ~10 minutes (Roelofs and Kamphuis, 2009), a real cloud could undergo 12 droplet cycles over the course of the experiments herein, implying a more continuous source of fresh interstitial VOCs than was recreated in our bulk-phase experiments. The bulk phase also limits gas exchange by eliminating droplet surface area at which exchange takes place: this lack of droplet surface area and attendant gas exchange may suppress both precursor absorption and volatile product evaporation (although drying before AMS analysis may offset the latter effect). The effect of evaporative cycling on aqSOA is a focus of current research.

In all, the bulk-aqueous/AMS analytical method is expected to lose a large and variable fraction of volatile oxidation products, the amount of which is highly dependent on the oxidation precursors and the volatility of their dominant products and is assumed to mimic the behavior of evaporating cloud droplets in the real atmosphere. Loss mechanisms may include a) evaporative loss during diffusion drying (Lee et al. 2011a), and b) evaporative loss during drying as the particle beam enters the high vacuum in the AMS (Zelenyuk et al., 2006). Mechanism a) might be more atmospherically relevant than b), but the current dataset cannot determine the contributions of each of these mechanisms to organic evaporative loss.

Also, while the continuously-mixed bulk solution methodology might prevent the phase separation observed in atmospheric aerosol water (e.g. organic shells, etc. which may change water evaporation and/or solute interaction and therefore reactivity), this effect is not thought to be important in cloud-relevant concentrations, where relative dilution leads to homogeneous mixing (Marcolli and Peter, 2005; Shiraiwa et al., 2013; Ziemann, 2010; Zuend et al., 2008). Under the assumption that the drying method used herein resemble those in the real atmosphere, the AMS does capture evaporated-cloud-relevant particulate organics.

CONCLUSIONS

This work explores how photooxidation influences ambient cloud water organic mass, oxidation state, and reaction regimes (such as functionalization versus fragmentation), and investigates relationships between oxidative progression and solution characteristics such as oxidation level (O:C) and initial total organic carbon (TOC). Unaltered ambient cloud water and 'biogenically influenced' ambient cloud water (via addition of pinonic acid) were photo-oxidized using UVC light and H_2O_2 (to form OH), atomized, and dried to simulate the formation of aqSOA from clouds; these experiments are among the first to quantify organic mass production in ambient cloud water and employ the most atmospherically relevant oxidant concentrations to date.

All ambient samples (except the heavily oxidized T2) gained carbonyl, then organic acid fragments; two of the five samples increased in sulfate-normalized organic mass (to a maximum of 110-140% of the t=0 value). All samples eventually lost organic mass (reaching 60-80% of their initial values), which is attributed to formation of volatile products in some cases ('Functionalization-Dominant Regime 1' evidenced by increasing 'formic acid' fragment and sustained increases in CO_2^+) and molecular decomposition leading to loss of oxidized functional groups in others ('Fragmentation-Dominant Regime 2'; CO_2^+, $C_2H_3O^+$,

O:C, and total organic mass decrease simultaneously); Regime 1 had significantly higher pH than Regime 2, and generally (though not significantly) higher initial total organic carbon, consistent with literature results showing formation of more functionalized products in higher-concentration solutions. The rate of aqSOA production in unaltered cloud water decreases as oxygenation increases, until organic mass loss beginning at a consistent value of O:C > 0.61 ± 0.05 and $f44$ > 0.23 ± 0.03 ($f43$ < 0.08 ± 0.02). This implies that there may be a parameterizable 'maximum oxidation level' for cloud water above which organic molecule fragmentation is dominant; however, we were unable to further mathematically describe the relationship between aqSOA production/loss rate and oxidation level. The consistency of this 'maximum oxidation level' within the Mt. Tai cloud water should prompt further investigation of cloud samples with varying composition and concentration. If widely applicable, such a parameterization would contribute greatly to the understanding and modeling of the secondary organic aerosols that contribute to so many important health, environmental, and climate effects. Lastly, addition of TOC in the form of pinonic acid to an ambient sample (meant to simulate interstitial biogenic precursor absorption) appeared to prevent organic mass loss and foster carbonyl formation, rendering the un-altered experiments herein lower-bound estimations of aqSOA formation in photooxidized clouds.

ACKNOWLEDGMENTS

Collection of Mt. Tai cloud samples was funded by NSF Grant ATM-0711102. Thanks to Taehyoung Lee and Xinhua Shen for collecting the Mt. Tai cloud samples used in this study, and Tao Wang, Wenxing Wang, and Xinfeng Wang for their help and partnership in planning the Mt. Tai cloud sampling campaign.

REFERENCES

456 Aljawhary, D., Zhao, R., Lee, A.K.Y., Wang, C. and Abbatt, J.P.D. 2016. Kinetics,
457 Mechanism, and Secondary Organic Aerosol Yield of Aqueous Phase Photo-oxidation of
458 α-Pinene OxidationProducts. The Journal of Physical Chemistry A 120(9), pp. 1395–1407.

459 Anastasio, C., Faust, B. C. and Allen, J. M.: Aqueous phase photochemical formation of
460 hydrogen peroxide in authentic cloud waters, J. Geophys. Res., 99(D4), 8231,
461 doi:10.1029/94JD00085, 1994.

462 Arakaki, T. and Faust, B. C.: Sources, sinks, and mechanisms of hydroxyl radical (• OH)
463 photoproduction and consumption in authentic acidic continental cloud waters from
464 Whiteface Mountain, New York: The role of the Fe(r) (r = II, III) photochemical cycle, J.
465 Geophys. Res., 103(D3), 3487, doi:10.1029/97JD02795, 1998.

466 Atkinson, R. and Arey, J.: Atmospheric degradation of volatile organic compounds., Chem.
467 Rev., 103(12), 4605–38, doi:10.1021/cr0206420, 2003.

468 Blando, J. D. and Turpin, B. J.: Secondary organic aerosol formation in cloud and fog
469 droplets: a literature evaluation of plausibility, Atmos. Environ., 34(10), 1623–1632,
470 doi:10.1016/S1352-2310(99)00392-1, 2000.

471 Bleier, D. B. and Elrod, M. J.: Kinetics and Thermodynamics of Atmospherically Relevant
472 Aqueous Phase Reactions of α-Pinene Oxide, J. Phys. Chem. A, 117(20), 4223–4232,
473 2013.

474 Boris, A. J., Desyaterik, Y. and Collett, J. L.: How do components of real cloud water affect
475 aqueous pyruvate oxidation?, Atmos. Res., 143, 95–106,
476 doi:10.1016/j.atmosres.2014.02.004, 2014.

477 Chang, J. L. and Thompson, J. E.: Characterization of colored products formed during
478 irradiation of aqueous solutions containing H2O2 and phenolic compounds, Atmos.

Environ., 44(4), 541–551, doi:10.1016/j.atmosenv.2009.10.042, 2010.

Chen, J., Griffin, R. J., Grini, A. and Tulet, P.: Modeling secondary organic aerosol formation through cloud processing of organic compounds, Atmos. Chem. Phys., 7(20), 5343–5355, doi:10.5194/acp-7-5343-2007, 2007.

Chhabra, P. S., Ng, N. L., Canagaratna, M. R., Corrigan, A. L., Russell, L. M., Worsnop, D. R., Flagan, R. C. and Seinfeld, J. H.: Elemental composition and oxidation of chamber organic aerosol, Atmos. Chem. Phys., 11(17), 8827–8845, doi:10.5194/acp-11-8827-2011, 2011.

Collett, J. L., Daube, B. C., Gunz, D. and Hoffmann, M. R.: Intensive studies of Sierra Nevada cloudwater chemistry and its relationship to precursor aerosol and gas concentrations, Atmos. Environ. Part A. Gen. Top., 24(7), 1741–1757, 1990.

Decarlo, P. F., Kimmel, J. R., Trimborn, A., Northway, M. J., Jayne, J. T., Aiken, A. C., Gonin, M., Fuhrer, K., Horvath, T., Docherty, K. S., Worsnop, D. R. and Jimenez, J. L.: Field-deployable, high-resolution, time-of-flight aerosol mass spectrometer., Anal. Chem., 78(24), 8281–9, doi:10.1021/ac061249n, 2006.

Deguillaume, L., Leriche, M. and Chaumerliac, N.: Impact of radical versus non-radical pathway in the Fenton chemistry on the iron redox cycle in clouds., Chemosphere, 60(5), 718–24, doi:10.1016/j.chemosphere.2005.03.052, 2005.

Ervens, B., George, C., Williams, J. E., Buxton, G. V., Salmon, G. A., Bydder, M., Wilkinson, F., Dentener, F., Mirabel, P., Wolke, R. and Herrmann, H.: CAPRAM 2.4 (MODAC mechanism): An extended and condensed tropospheric aqueous phase mechanism and its application, J. Geophys. Res., 108(D14), 4426, doi:10.1029/2002JD002202, 2003a.

Ervens, B., Gligorovski, S. and Herrmann, H.: Temperature-dependent rate constants for hydroxyl radical reactions with organic compounds in aqueous solutions, Phys. Chem. Chem. Phys., 5(9), 1811–1824, doi:10.1039/b300072a, 2003b.

Ervens, B. and Volkamer, R.: Glyoxal processing by aerosol multiphase chemistry: towards a kinetic modeling framework of secondary organic aerosol formation in aqueous particles, Atmos. Chem. Phys., 10(17), 8219–8244, doi:10.5194/acp-10-8219-2010, 2010.

Fischer, M. and Warneck, P.: Photodecomposition of Nitrite and Undissociated Nitrous Acid in Aqueous Solution, J. Phys. Chem., 100(48), 18749–18756, doi:10.1021/jp961692+, 1996.

Fornaro, A. and Gutz, I. G. R.: Wet deposition and related atmospheric chemistry in the São Paulo metropolis, Brazil: Part 2—contribution of formic and acetic acids, Atmos. Environ., 37(1), 117–128, 2003.

Fu, T. M., Jacob, D. J., Wittrock, F., Burrows, J. P., Vrekoussis, M. and Henze, D. K.: Global budgets of atmospheric glyoxal and methylglyoxal, and implications for formation of secondary organic aerosols, J. Geophys. Res., 113(D15), D15303, doi:10.1029/2007JD009505, 2008.

Galloway, M. M., Loza, C. L., Chhabra, P. S., Chan, A. W. H., Yee, L. D., Seinfeld, J. H. and Keutsch, F. N.: Analysis of photochemical and dark glyoxal uptake: Implications for SOA formation, Geophys. Res. Lett., 38(17), n/a–n/a, doi:10.1029/2011GL048514, 2011.

George, I. J. and Abbatt, J. P. D.: Chemical evolution of secondary organic aerosol from OH-initiated heterogeneous oxidation, Atmos. Chem. Phys., 10(12), 5551–5563, doi:10.5194/acp-10-5551-2010, 2010.

Graedel, T. E. and Goldberg, K. I.: Kinetic studies of raindrop chemistry: 1. Inorganic and

525 organic processes, J. Geophys. Res., 88(C15), 10865, doi:10.1029/JC088iC15p10865,
526 1983.

527 Graedel, T. E. and Weschler, C. J.: Chemistry within aqueous atmospheric aerosols and
528 raindrops, Rev. Geophys., 19(4), 505, doi:10.1029/RG019i004p00505, 1981.

529 Guzman, M. I., Colussi, A. J. and Hoffmann, M. R.: Photoinduced oligomerization of
530 aqueous pyruvic acid., J. Phys. Chem. A, 110(10), 3619–26, doi:10.1021/jp056097z, 2006.

531 De Haan, D. O., Corrigan, A. L., Tolbert, M. A., Jimenez, J. L., Wood, S. E. and Turley, J. J.:
532 Secondary organic aerosol formation by self-reactions of methylglyoxal and glyoxal in
533 evaporating droplets., Environ. Sci. Technol., 43(21), 8184–90, doi:10.1021/es902152t,
534 2009.

535 El Haddad, I., Nieto-Gligorovski, L., Michaud, V., Temime-Roussel, B., Quivet, E.,
536 Marchand, N., Sellegri, K. and Monod, A.: In-cloud processes of methacrolein under
537 simulated conditions – Part 2: Formation of secondary organic aerosol, Atmos. Chem.
538 Phys., 9(14), 5107–5117, doi:10.5194/acp-9-5107-2009, 2009.

539 Heald, C. L., Jacob, D. J., Park, R. J., Russell, L. M., Huebert, B. J., Seinfeld, J. H., Liao, H.
540 and Weber, R. J.: A Large Organic Aerosol Source in the Free Troposphere Missing from
541 Current Models, 2005.

542 Heald, C. L., Kroll, J. H., Jimenez, J. L., Docherty, K. S., DeCarlo, P. F., Aiken, A. C., Chen,
543 Q., Martin, S. T., Farmer, D. K. and Artaxo, P.: A simplified description of the evolution
544 of organic aerosol composition in the atmosphere, Geophys. Res. Lett., 37(8), L08803,
545 doi:10.1029/2010GL042737, 2010.

546 Herrmann, H., Hoffmann, D., Schaefer, T., Bräuer, P. and Tilgner, A.: Tropospheric aqueous-
547 phase free-radical chemistry: radical sources, spectra, reaction kinetics and prediction

548 tools., Chemphyschem, 11(18), 3796–822, doi:10.1002/cphc.201000533, 2010.

549 Jacob, D. J.: Chemistry of OH in remote clouds and its role in the production of formic acid
550 and peroxymonosulfate, J. Geophys. Res., 91(D9), 9807, doi:10.1029/JD091iD09p09807,
551 1986.

552 Jang, M.: Newly characterized products and composition of secondary aerosols from the
553 reaction of α-pinene with ozone, Atmos. Environ., 33(3), 459–474, doi:10.1016/S1352-
554 2310(98)00222-2, 1999.

555 Kanakidou, M., Seinfeld, J. H., Pandis, S. N., Barnes, I., Dentener, F. J., Facchini, M. C., Van
556 Dingenen, R., Ervens, B., Nenes, a., Nielsen, C. J., Swietlicki, E., Putaud, J. P., Balkanski,
557 Y., Fuzzi, S., Horth, J., Moortgat, G. K., Winterhalter, R., Myhre, C. E. L., Tsigaridis, K.,
558 Vignati, E., Stephanou, E. G. and Wilson, J.: Organic aerosol and global climate
559 modelling: a review, Atmos. Chem. Phys., 5(4), 1053–1123, doi:10.5194/acp-5-1053-2005,
560 2005.

561 Kawamura, K., IMAI, Y. and BARRIE, L.: Photochemical production and loss of organic
562 acids in high Arctic aerosols during long-range transport and polar sunrise ozone depletion
563 events, Atmos. Environ., 39(4), 599–614, doi:10.1016/j.atmosenv.2004.10.020, 2005.

564 Kawamura, K., Matsumoto, K., Tachibana, E. and Aoki, K.: Low molecular weight (C1–C10)
565 monocarboxylic acids, dissolved organic carbon and major inorganic ions in alpine snow
566 pit sequence from a high mountain site, central Japan, Atmos. Environ., 62, 272–280, 2012.

567 Kroll, J. H., Donahue, N. M., Jimenez, J. L., Kessler, S. H., Canagaratna, M. R., Wilson, K.
568 R., Altieri, K. E., Mazzoleni, L. R., Wozniak, A. S., Bluhm, H., Mysak, E. R., Smith, J. D.,
569 Kolb, C. E. and Worsnop, D. R.: Carbon oxidation state as a metric for describing the
570 chemistry of atmospheric organic aerosol., Nat. Chem., 3(2), 133–9,

571 doi:10.1038/nchem.948, 2011.

572 Lambe, A. T., Onasch, T. B., Massoli, P., Croasdale, D. R., Wright, J. P., Ahern, A. T.,
573 Williams, L. R., Worsnop, D. R., Brune, W. H. and Davidovits, P.: Laboratory studies of
574 the chemical composition and cloud condensation nuclei (CCN) activity of secondary
575 organic aerosol (SOA) and oxidized primary organic aerosol (OPOA), Atmos. Chem.
576 Phys., 11(17), 8913–8928, doi:10.5194/acp-11-8913-2011, 2011.

577 Lee, A. K. Y., Hayden, K. L., Herckes, P., Leaitch, W. R., Liggio, J., Macdonald, A. M. and
578 Abbatt, J. P. D.: Characterization of aerosol and cloud water at a mountain site during
579 WACS 2010: secondary organic aerosol formation through oxidative cloud processing,
580 Atmos. Chem. Phys., 12(15), 7103–7116, doi:10.5194/acp-12-7103-2012, 2012.

581 Lee, A. K. Y., Herckes, P., Leaitch, W. R., Macdonald, A. M. and Abbatt, J. P. D.: Aqueous
582 OH oxidation of ambient organic aerosol and cloud water organics: Formation of highly
583 oxidized products, Geophys. Res. Lett., 38(11), n/a–n/a, doi:10.1029/2011GL047439,
584 2011a.

585 Lee, A. K. Y., Zhao, R., Gao, S. S. and Abbatt, J. P. D.: Aqueous-phase OH oxidation of
586 glyoxal: application of a novel analytical approach employing aerosol mass spectrometry
587 and complementary off-line techniques., J. Phys. Chem. A, 115(38), 10517–26,
588 doi:10.1021/jp204099g, 2011b.

589 Lignell, H., Epstein, S., Marvin, M. and et al. 2013. Experimental and theoretical study of
590 aqueous cis-pinonic acid photolysis. The Journal of Physical Chemistry A 2013 117 (48),
591 12930-12945 DOI: 10.1021/jp4093018

592 Lim, Y. B., Tan, Y., Perri, M. J., Seitzinger, S. P. and Turpin, B. J.: Aqueous chemistry and
593 its role in secondary organic aerosol (SOA) formation, Atmos. Chem. Phys., 10(21),

10521–10539, doi:10.5194/acp-10-10521-2010, 2010.

Liu, J., Horowitz, L. W., Fan, S., Carlton, A. G. and Levy, H.: Global in-cloud production of secondary organic aerosols: Implementation of a detailed chemical mechanism in the GFDL atmospheric model AM3, J. Geophys. Res., 117(D15), D15303, doi:10.1029/2012JD017838, 2012a.

Liu, J., Zhang, X., Parker, E. T., Veres, P. R., Roberts, J. M., de Gouw, J. A., Hayes, P. L., Jimenez, J. L., Murphy, J. G., Ellis, R. A., Huey, L. G. and Weber, R. J.: On the gas-particle partitioning of soluble organic aerosol in two urban atmospheres with contrasting emissions: 2. Gas and particle phase formic acid, J. Geophys. Res. Atmos., 117(D21), n/a–n/a, doi:10.1029/2012JD017912, 2012b.

Liu, Y., El Haddad, I., Scarfogliero, M., Nieto-Gligorovski, L., Temime-Roussel, B., Quivet, E., Marchand, N., Picquet-Varrault, B. and Monod, A.: In-cloud processes of methacrolein under simulated conditions – Part 1: Aqueous phase photooxidation, Atmos. Chem. Phys., 9(14), 5093–5105, doi:10.5194/acp-9-5093-2009, 2009.

Loeffler, K. W., Koehler, C. A., Paul, N. M. and De Haan, D. O.: Oligomer Formation in Evaporating Aqueous Glyoxal and Methyl Glyoxal Solutions, Environ. Sci. Technol., 40(20), 6318–6323, doi:10.1021/es060810w, 2006.

Löflund, M., Kasper-Giebl, A., Schuster, B., Giebl, H., Hitzenberger, R. and Puxbaum, H.: Formic, acetic, oxalic, malonic and succinic acid concentrations and their contribution to organic carbon in cloud water., 2002.

Malm, W. C., Barna, M. G., Beem, K. B., Carrico, C. M., Collett Jr., J. L., Day, D. E., Gebhart, K. A., Hand, J. L., Kreidenweis, S. M., Lee, T., Levin, E. J. T., McDade, C. E., McMeeking, G. R., Molenar, J. V., Raja, S., Rodriguez, M. A., Schichtel, B. A.,

617 Schwandner, F. M., Sullivan, A. P. and Taylor, C.: Rocky Mountain Atmospheric
618 Nitrogen and Sulfur Study, Fort Collins, CO., 2009.

619 McLafferty, F. W. and Turecek, F.: Interpretation of Mass Spectra, 4th ed., University
620 Science Books, Herndon, VA., 1993.

621 Monod, A., Chebbi, A., Durand-Jolibois, R. and Carlier, P.: Oxidation of methanol by
622 hydroxyl radicals in aqueous solution under simulated cloud droplet conditions, Atmos.
623 Environ., 34(29-30), 5283–5294, doi:10.1016/S1352-2310(00)00191-6, 2000.

624 Monod, A., Chevallier, E., Durandjoliboi, R., Doussin, J., Picquet-Varrault, B. and Carlier, P.:
625 Photooxidation of methylhydroperoxide and ethylhydroperoxide in the aqueous phase
626 under simulated cloud droplet conditions, Atmos. Environ., 41(11), 2412–2426,
627 doi:10.1016/j.atmosenv.2006.10.006, 2007.

628 Müller, L., Reinnig, M.-C., Naumann, K. H., Saathoff, H., Mentel, T. F., Donahue, N. M. and
629 Hoffmann, T.: Formation of 3-methyl-1,2,3-butanetricarboxylic acid via gas phase
630 oxidation of pinonic acid – a mass spectrometric study of SOA aging, Atmos. Chem. Phys.,
631 12(3), 1483–1496, doi:10.5194/acp-12-1483-2012, 2012.

632 Ng, N. L., Canagaratna, M. R., Jimenez, J. L., Chhabra, P. S., Seinfeld, J. H. and Worsnop, D.
633 R.: Changes in organic aerosol composition with aging inferred from aerosol mass spectra,
634 Atmos. Chem. Phys., 11(13), 6465–6474, doi:10.5194/acp-11-6465-2011, 2011.

635 Ng, N. L., Canagaratna, M. R., Zhang, Q., Jimenez, J. L., Tian, J., Ulbrich, I. M., Kroll, J. H.,
636 Docherty, K. S., Chhabra, P. S., Bahreini, R., Murphy, S. M., Seinfeld, J. H., Hildebrandt,
637 L., Donahue, N. M., DeCarlo, P. F., Lanz, V. a., Prévôt, a. S. H., Dinar, E., Rudich, Y.
638 and Worsnop, D. R.: Organic aerosol components observed in Northern Hemispheric
639 datasets from Aerosol Mass Spectrometry, Atmos. Chem. Phys., 10(10), 4625–4641,

doi:10.5194/acp-10-4625-2010, 2010.

Nozière, B., Barnes, I. and Becker, K. H.: Product study and mechanisms of the reactions of α-pinene and of pinonaldehyde with OH radicals, J. Geophys. Res., 104(D19), 23645, doi:10.1029/1999JD900778, 1999.

Oturan, M. A., Peiroten, J., Chartrin, P. and Acher, A. J.: Complete Destruction of p - Nitrophenol in Aqueous Medium by Electro-Fenton Method, Environ. Sci. Technol., 34(16), 3474–3479, doi:10.1021/es990901b, 2000.

van Pinxteren, D., Plewka, A., Hofmann, D., Müller, K., Kramberger, H., Svrcina, B., Bächmann, K., Jaeschke, W., Mertes, S., Collett, J. L. and Herrmann, H.: Schmücke hill cap cloud and valley stations aerosol characterisation during FEBUKO (II): Organic compounds, Atmos. Environ., 39(23-24), 4305–4320, doi:10.1016/j.atmosenv.2005.02.014, 2005.

Schurman, M. I.: Characteristics, Sources, and Formation of Organic Aerosols in the Rocky Mountains, Colorado State University, Fort Collins, Colorado., 2014.

Shen, X.: Aqueous Phase Sulfate Production in Clouds at Mt. Tai in Eastern China, Colorado State University., 2011.

Takegawa, N., Miyakawa, T., Kawamura, K. and Kondo, Y.: Contribution of selected dicarboxylic and omega-oxocarboxylic acids in ambient aerosol to the m/z 44 signal of an Aerodyne aerosol mass spectrometer, Aerosol Sci. Technol., 41, 418–437, 2007.

Tan, Y., Carlton, A. G., Seitzinger, S. P. and Turpin, B. J.: SOA from methylglyoxal in clouds and wet aerosols: Measurement and prediction of key products, Atmos. Environ., 44(39), 5218–5226, doi:10.1016/j.atmosenv.2010.08.045, 2010.

662 Tan, Y., Lim, Y. B., Altieri, K. E., Seitzinger, S. P. and Turpin, B. J.: Mechanisms leading to
663 oligomers and SOA through aqueous photooxidation: insights from OH radical oxidation
664 of acetic acid and methylglyoxal, Atmos. Chem. Phys., 12(2), 801–813, doi:10.5194/acp-
665 12-801-2012, 2012.

666 Tan, Y., Perri, M. J., Seitzinger, S. P. and Turpin, B. J.: Effects of precursor concentration
667 and acidic sulfate in aqueous glyoxal-OH radical oxidation and implications for secondary
668 organic aerosol., Environ. Sci. Technol., 43(21), 8105–12, doi:10.1021/es901742f, 2009.

669 Tsigaridis, K. and Kanakidou, M.: Global modelling of secondary organic aerosol in the
670 troposphere: a sensitivity analysis, Atmos. Chem. Phys., 3(5), 1849–1869,
671 doi:10.5194/acp-3-1849-2003, 2003.

672 Valverde-Canossa, J., Wieprecht, W., Acker, K. and Moortgat, G. K.: H2O2 and organic
673 peroxide measurements in an orographic cloud: The FEBUKO experiment, Atmos.
674 Environ., 39(23-24), 4279–4290, doi:10.1016/j.atmosenv.2005.02.040, 2005.

675 Volkamer, R. M., Ziemann, P. J. and Molina, M. J.: Secondary Organic Aerosol Formation
676 from Acetylene (C2H2): seed effect on SOA yields due to organic photochemistry in the
677 aerosol aqueous phase, Atmos. Chem. Phys., 9(6), 1907–1928, doi:10.5194/acp-9-1907-
678 2009, 2009.

679 Wang, Y., Zhuang, G., Chen, S., An, Z. and Zheng, A.: Characteristics and sources of formic,
680 acetic and oxalic acids in PM2.5 and PM10 aerosols in Beijing, China, Atmos. Res., 84(2),
681 169–181, doi:10.1016/j.atmosres.2006.07.001, 2007.

682 Weschler, C. J., Mandich, M. L. and Graedel, T. E.: Speciation, photosensitivity, and
683 reactions of transition metal ions in atmospheric droplets, J. Geophys. Res., 91(D4), 5189,
684 doi:10.1029/JD091iD04p05189, 1986.

685 Yu, J., III, D. R. C., Griffin, R. J., Flagan, R. C. and Seinfeld, J. H.: Gas-Phase Ozone
686 Oxidation of Monoterpenes: Gaseous and Particulate Products, J. Atmos. Chem., 34(2),
687 207–258, doi:10.1023/A:1006254930583, 1999.

688 Zellner, R., Exner, M. and Herrmann, H.: Absolute OH quantum yields in the laser photolysis
689 of nitrate, nitrite and dissolved H2O2 at 308 and 351 nm in the temperature range 278?353
690 K, J. Atmos. Chem., 10(4), 411–425, doi:10.1007/BF00115783, 1990.

691

692

693

694

695

696

697

698

699

700

701

702 **Table 1:** Initial total organic carbon (TOC, μg/L) in the given ambient cloud water sample
703 (T#). *Due to low sample volume, T1 is a combination of three cloud samples; TOC and pH
704 are estimated using averages of the three samples and assuming equal volumes.

	T1*	**T2**	**T3**	**T4**	**T6PA**	**T7/7PA**
TOC	~20	24.1	2.86	1.73	9.17	6.40/10.06
pH	~5.49	3.32	6.37	4.74	~3.7	4.58/~3.7

Figure Captions

Figure 1: Schematic of photoreactor experimental setup. Circles with black triangles indicate pumps.

Figure 2: Timelines of *f*44 (red), normalized (to t=0) Org/SO_4 (green), and O:C (blue) for T1, T2, T3, T4-1, and T7 aqueous photo-oxidations. Uncertainties (not plotted): one standard deviation equals 28% of the value, from propagation of 20% AMS quantification error through the indicated calculations. Experiment time approximates ambient oxidation time as discussed in Section 2.3.

Figure 3: Timelines of (left axes) fragment ratios normalized to the t=0 value and (right axes) the mass concentration of the 'formic acid' fragment for T1-4, T7, and T7PA. Uncertainties (not plotted): one standard deviation equals 28% of the value, from propagation of 20% AMS quantification error through the indicated calculations.

Figure 4: van Krevelen diagram showing (left) T1, 3, & 4 full photo-oxidations and (right) T2, 7, & 7PA, colored by time during experiment. Dashed red lines: Estimated oxidation state, OS_c=2*O:C-H:C (Kroll et al., 2011). Red and blue lines indicate the region usually inhabited by ambient data in the *f43* vs *f44* plot, as transposed to van Krevelen space using the empirical parameterization of *f*43 vs H:C and *f*44 vs O:C for ambient and chamber OA (Ng et al., 2010); grey lines represent 10% error. Linear fits: T1: m = -0.28, r^2 = 0.89; T2: m = 0.25, r^2 = 0.32; T3: m = -0.28, r^2 = 0.64; T4: m = -0.51 (see text), r^2 = 0.46; T7: m = -0.32 (see text), r^2 = 0.14; T7PA: m = -0.45, r^2 = 0.26.

Figure 5: Initial concentrations of the given cloud water constituents for given sample regimes. Units are, from left to right: Cl-Ca, HCHO, & S(IV) (μN); TC-TOC (ppm); Fe & Mn (μg/L). Error bars are standard deviations where data from multiple samples of the same regime were averaged. T2 consists of only one sample, so error bars are omitted.

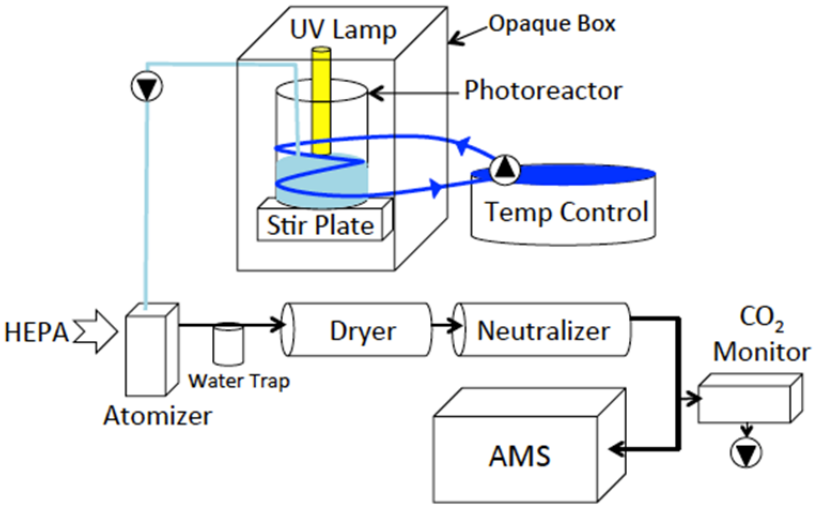

Fig.1

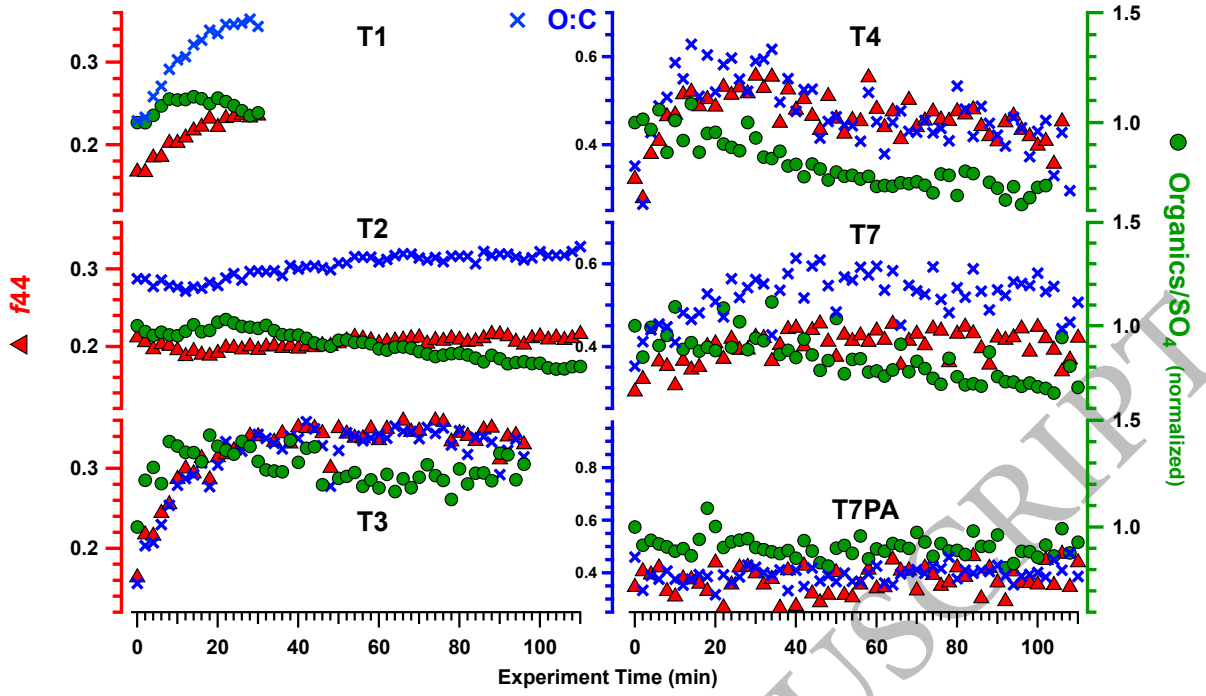

751

752

753

754

755

756

757

758

759

760

761

762 Fig. 2

763

764

765

766

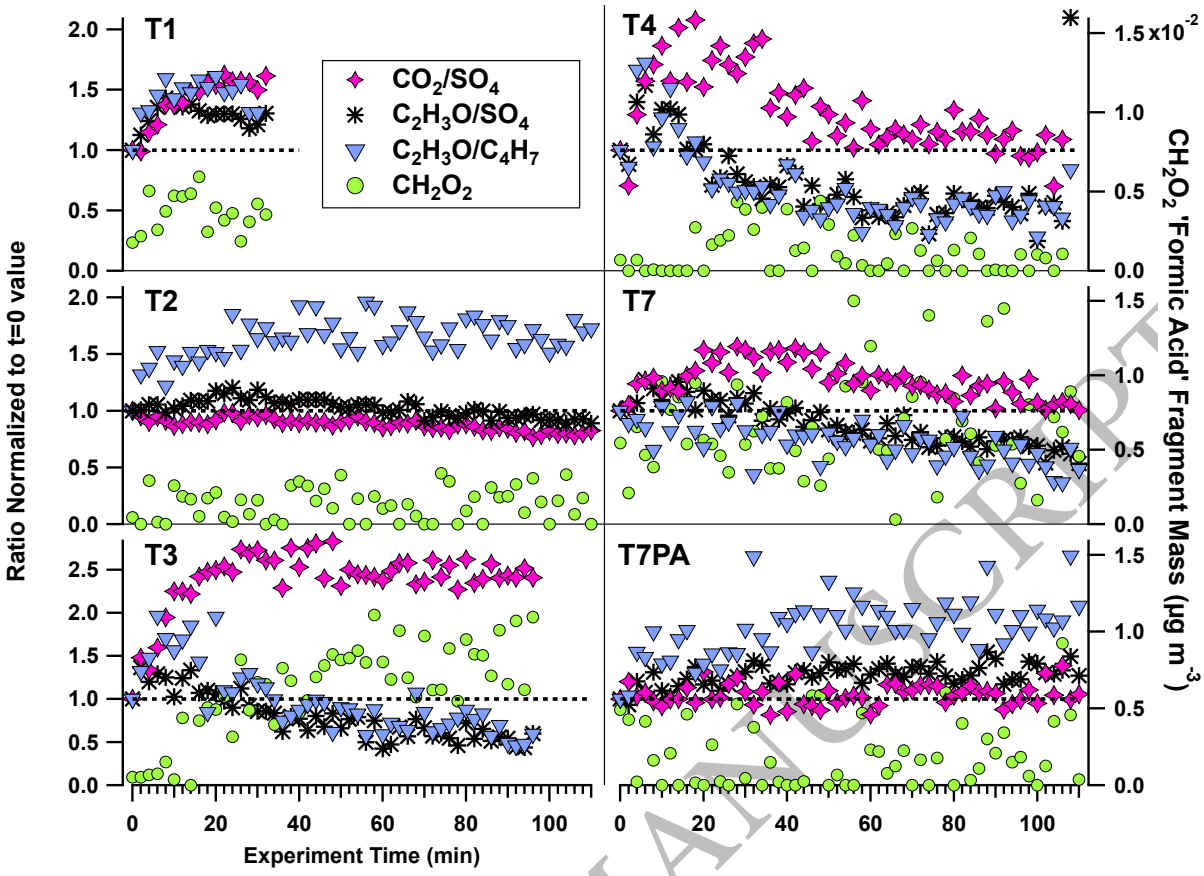

Fig. 3

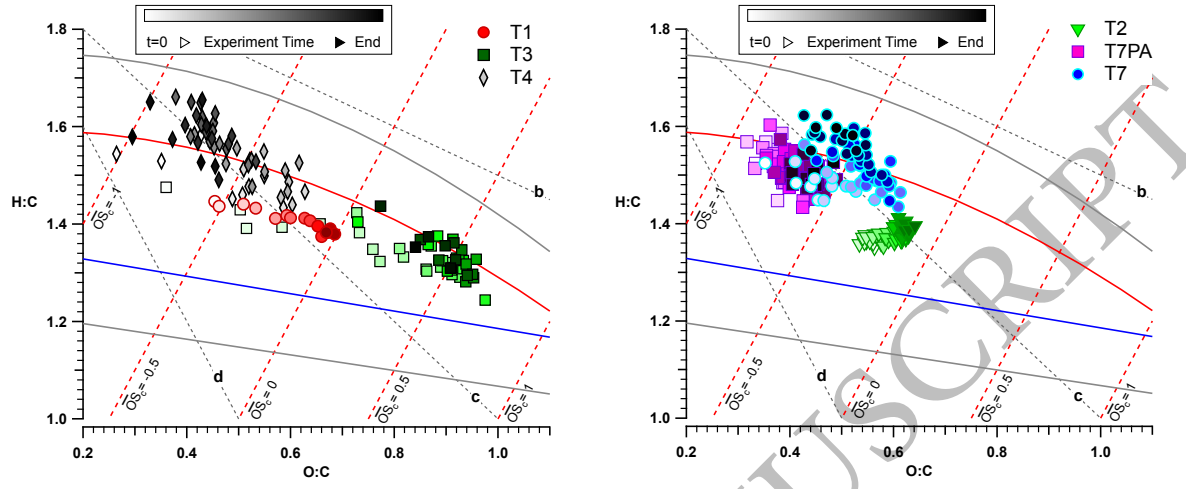

Fig. 4

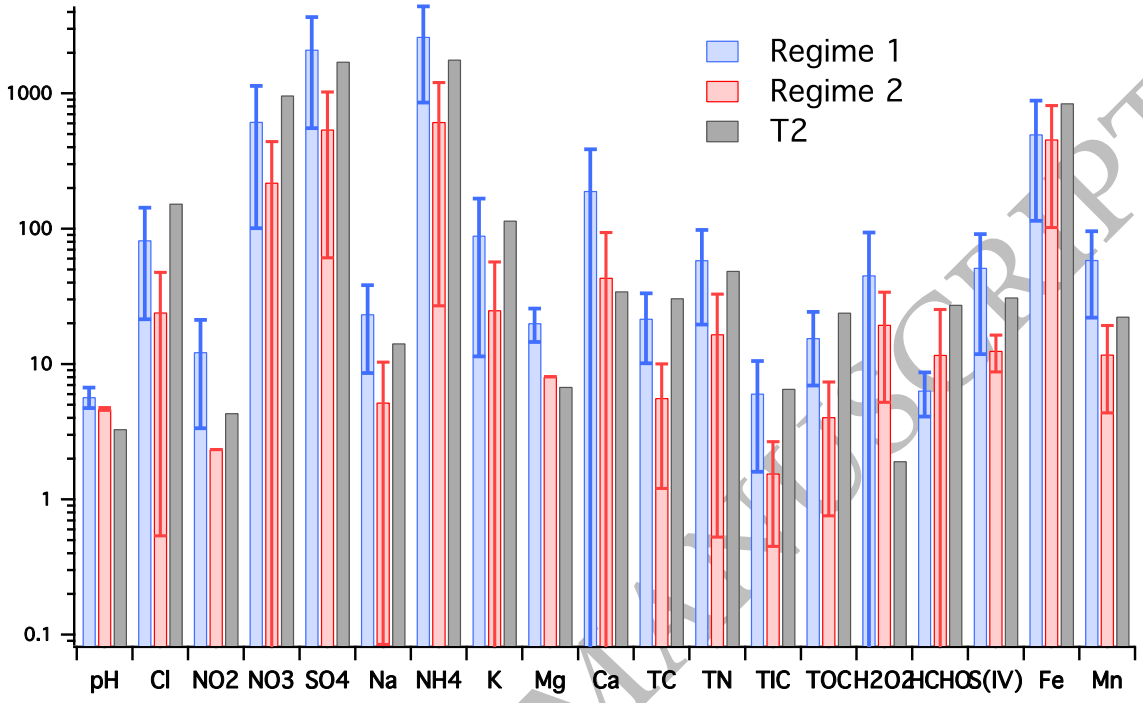

Fig. 5